

What is a chemostat?

Insights from hybrid dynamics and stochastic thermodynamics

Benedikt Remlein,^{1, a)} Massimiliano Esposito,^{1, b)} and Francesco Avanzini^{2, c)}

¹⁾*Complex Systems and Statistical Mechanics, Department of Physics and Materials Science, University of Luxembourg, 30 Avenue des Hauts-Fourneaux, L-4362 Esch-sur-Alzette, Luxembourg*

²⁾*Department of Chemical Sciences, University of Padova, Via F. Marzolo, 1, I-35131 Padova, Italy*

(Dated: 25 February 2025)

At the microscopic scale, open chemical reaction networks are described by stochastic reactions that follow mass-action kinetics and are coupled to chemostats. We show that closed chemical reaction networks – with specific stoichiometries imposed by mass-action kinetics – behave like open ones in the limit where the abundances of a subset of species become macroscopic, thus playing the role of chemostats. We prove that this limit is thermodynamically consistent by recovering the local detailed balance condition of open chemical reaction networks and deriving the proper expression of the entropy production rate. In particular, the entropy production rate features two contributions: one accounting for the dissipation of the stochastic reactions, the other for the dissipation of continuous reactions controlling the chemostats. Finally, we illustrate our results for two prototypical examples.

I. INTRODUCTION

Many complex processes in biosystems and synthetic chemistry arise from underlying open chemical reaction networks (CRNs) maintained out of equilibrium.^{1,2} The energetic cost that enables CRNs to stay out of equilibrium is harnessed from the environment via exchanges of chemical species.³ High-energy species are harvested and converted into low-energy species released back into the environment to power reactions that would otherwise equilibrate.^{4,5} For instance, in biosystems, cellular metabolism converts glucose into carbon dioxide to continuously produce energetic mediator molecules, e.g., adenosine triphosphate.⁶ Similarly, in synthetic chemistry, different high-energy-species-to-low-energy-species reactions are used to, for instance, produce a directional motion in artificial molecular motors or form energetically unfavorable assemblies.^{7,8}

In recent years, rigorous theoretical frameworks have been developed to explain such complex processes, often modeling the environment in terms of chemostats, i.e., infinitely large reservoirs of chemical species that remain unaffected by chemical reactions, but can evolve as a result of some (externally imposed) driving protocol. From a dynamical standpoint, these theories have been used, for instance, to prove the emergence of oscillations and chaos.^{9,10} Furthermore, driving the chemostats has been shown to (potentially) lead to a highly nonlinear response of the reaction currents,^{11–13} but it cannot, in general, invert them.¹⁴ Correspondingly, thermodynamic theories have been derived to quantify the energetic cost of maintaining CRNs out of equilibrium independently of whether reactions are described as stochastic^{15–17} (microscopic scale) or deterministic^{18–21} (macroscopic scale) events. These theories have been used to quantify the

cost of maintaining coherent oscillations,^{22,23} of powering chemical growth,^{24,25} as well as to study the efficiency of central metabolism.^{4,26} They also define thermodynamic speed limits.^{27,28}

While the notion of chemostats has proven invaluable in these frameworks, recent studies have begun exploring ways to move beyond it. For instance, the emergence of oscillations in a specific CRN coupled to finite chemostats has been investigated at the microscopic scale,²⁹ while the thermodynamics of CRNs directly coupled to specific exchange processes, instead of chemostats, has been studied at the macroscopic scale.^{30,31} However, a rigorous explanation of the emergence of chemostats is still missing. In this paper, we bridge the gap between a closed description of CRNs, where all species have finite abundances, and an open one, where abundant species are treated as chemostats.

We focus on CRNs at the microscopic scale, where species abundances are quantified by molecule numbers and reactions are stochastic events following mass-action kinetics. We prove that the dynamics and thermodynamics of open CRNs (summarized in Sec. II) emerge from a partial macroscopic limit of closed CRNs with specific stoichiometries.

To do so, we use a large volume limit^{32–38} developed for hybrid CRNs (summarized in Sec. III) where high-abundant species, whose molecule numbers scale (linearly) with the volume, are mixed together with low-abundant species, whose molecule numbers do not scale with the volume. Crucially, this volume limit is based on the Wentzel–Kramers–Brillouin (WKB) ansatz,^{39–44} avoiding physical inconsistencies found in previous scalings.^{45,46} It leads to a hybrid dynamics. The low-abundant species are interconverted by reactions (called discrete reactions) still described in terms of stochastic events. The high-abundant species can be interconverted only by reactions (called continuous reactions) described in terms of deterministic events.

First, we show that the partial macroscopic limit can only be applied to CRNs satisfying specific stoichiometric conditions (in Eqs. (17) and (18)) imposed by mass-action kinetics (Sec. IV). When these conditions are met, the high-abundant

^{a)}Electronic mail: benedikt.remlein@uni.lu

^{b)}Electronic mail: massimiliano.esposito@uni.lu

^{c)}Electronic mail: francesco.avanzini@unipd.it

species become (in the large volume limit) chemostats. If there are no continuous reactions, the resulting chemostats are autonomous with constant concentrations (Subs. IV B). Otherwise, continuous reactions impose a deterministic evolution independent of the low-abundant species on chemostat concentrations (Subs. IV C), thus physically representing the (externally imposed) driving protocols used in the modeling of open CRNs.

Second, we prove that the partial macroscopic limit is thermodynamically consistent (Sec. V). On the one hand, it leads to the local detailed balance condition of open CRNs (Subs. V A). On the other hand, we derive the corresponding entropy production rate (Sec. V B) which results from the sum of two contributions. One contribution accounts for the dissipation of the discrete reactions corresponding to the entropy production rate of open CRNs and does not scale with the volume (Subs. V B 1). The other accounts for the dissipation of the continuous reactions and scales (linearly) with the volume (Subs. V B 2). In particular, the latter contribution physically quantifies the dissipation of the (externally imposed) protocols that manipulate chemostats and is always neglected in the modeling of open CRNs.

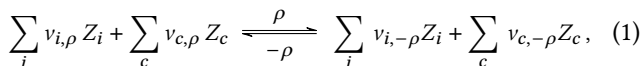
Finally, we illustrate our results for two prototypical examples (Sec. VI), one featuring a CRN without continuous reactions, while the other featuring a CRN with a continuous reaction.

We summarize and discuss our results in Sec. VII, where we also examine future perspectives.

II. CHEMICAL REACTION NETWORKS

Chemical reaction networks (CRNs) describe mixtures of reacting chemical species (labeled α) and an abundant non-reacting species called the solvent (labeled s). The solvent plays the role of a thermal and volume reservoir, maintaining the mixture temperature T and volume Ω constant. CRNs are said to be *open* when the abundances of some reacting species (labeled c) are controlled by unspecified external processes and thus act as *chemostats*. The other reacting species (labeled i) are called *internal* species. In the absence of chemostats, CRNs are said to be *closed*. In the following, we use n_α for the molecule number of species α and n_s for the molecule number of the solvent. The vectors $\mathbf{n}_i \equiv (\dots, n_i, \dots)$ and $[\mathbf{c}] \equiv (\dots, [c], \dots)$ specify the molecule numbers of the internal species and the concentrations of the chemostats, respectively. Note that the concentrations $[c]_t$ can evolve in time as a result of some driving protocol imposed by the external processes. In this case, chemostats are said to be *evolving*. Otherwise, if the concentrations $[c]_t$ are maintained constant by the external processes, chemostats are said to be *autonomous*.

Reactions (labeled $\rho \in \mathcal{R} \equiv \{\pm 1, \pm 2, \dots, n_r\}$) interconvert the reacting species and are described by the following chemical equation



where Z_α is the chemical symbol of species α , while $v_{\alpha,\rho}$ denotes its stoichiometric coefficient in reaction ρ . The net variation of molecule number of species α in reaction ρ is specified by

$$S_{\alpha,\rho} \equiv v_{\alpha,-\rho} - v_{\alpha,\rho}, \quad (2)$$

and we define the vectors $\mathbf{S}_{i,\rho} = (\dots, S_{i,\rho}, \dots)$ and $\mathbf{S}_{c,\rho} = (\dots, S_{c,\rho}, \dots)$ for the internal species and the chemostats, respectively. Note that reactions are assumed here to be reversible: for every forward reaction $\rho \in \mathcal{R}$, reaction $-\rho \in \mathcal{R}$ and denotes its backward counterpart.

The probability $P_t(\mathbf{n}_i)$ of there being \mathbf{n}_i molecules at time t follows the chemical master equation (CME),

$$\partial_t P_t(\mathbf{n}_i) = \sum_{\rho \in \mathcal{R}} \{R_\rho(\mathbf{n}_i - \mathbf{S}_{i,\rho} | [\mathbf{c}]_t) P_t(\mathbf{n}_i - \mathbf{S}_{i,\rho}) - R_\rho(\mathbf{n}_i | [\mathbf{c}]_t) P_t(\mathbf{n}_i)\}, \quad (3)$$

where the reaction rates are assumed to satisfy mass-action kinetics,¹⁵

$$R_\rho(\mathbf{n}_i | [\mathbf{c}]_t) \equiv \Omega k_\rho \prod_i \frac{n_i!}{(n_i - v_{i,\rho})!} \Omega^{v_{i,\rho}} \prod_c [c]_t^{v_{c,\rho}}, \quad (4)$$

with $k_\rho > 0$ being the kinetic rate constant of reaction ρ . The volume dependence in Eq. (4) guarantees the correct correspondence between stochastic and deterministic reaction rates in the macroscopic limit (i.e., for large molecule numbers of all species $\{n_\alpha\}$ and a large volume Ω , but with finite concentrations $\{n_\alpha/\Omega\}$).⁴⁷ Furthermore, we stress that mass-action kinetics is satisfied for elementary reactions in ideal dilute mixtures, namely, species are noninteracting and the solvent is much more abundant than all the other species. If reactions are not elementary or species interact, reaction rates might not satisfy mass-action kinetics. In this work, we consider only elementary reactions in ideal dilute mixtures. Finally, we stress that in the following we will use $R_\rho(\mathbf{n}_i)$ (resp. $R_\rho([\mathbf{c}]_t)$) for the rate of a reaction not involving (resp. involving only) chemostats, instead of the general symbol $R_\rho(\mathbf{n}_i | [\mathbf{c}]_t)$.

Thermodynamic consistency imposes that reaction rates (4) are related to the Gibbs free energy via the so-called local detailed balance condition,¹⁷

$$\ln \frac{R_\rho(\mathbf{n}_i | [\mathbf{c}]_t)}{R_{-\rho}(\mathbf{n}_i + \mathbf{S}_{i,\rho} | [\mathbf{c}]_t)} = -\{\Delta_\rho g(\mathbf{n}_i) + \boldsymbol{\mu}([\mathbf{c}]_t) \cdot \mathbf{S}_{c,\rho}\}. \quad (5)$$

Here, $\Delta_\rho g(\mathbf{n}_i) \equiv g(\mathbf{n}_i + \mathbf{S}_{i,\rho}) - g(\mathbf{n}_i)$ is the variation of the Gibbs free energy along reaction ρ due to the internal species and

$$g(\mathbf{n}_i) \equiv \sum_i \{(\mu_i^\circ - \ln n_s) n_i + \ln n_i!\}, \quad (6)$$

is the Gibbs free energy (given in units of temperature T times Boltzmann constant k_B) of ideal dilute mixtures with \mathbf{n}_i molecules of internal species, with μ_i° being the standard chemical potential of species i . On the other hand,

$\boldsymbol{\mu}([\mathbf{c}]_t) \cdot \mathbf{S}_{c,\rho}$ is the variation of the Gibbs free energy along reaction ρ due to the chemostats and

$$\boldsymbol{\mu}([\mathbf{c}]_t) \equiv \boldsymbol{\mu}_c^\circ + \ln([\mathbf{c}]_t/[s]), \quad (7)$$

is the vector of their chemical potentials, with $\boldsymbol{\mu}_c^\circ = (\dots, \mu_c^\circ, \dots)$ being their standard chemical potentials, $\ln[\mathbf{c}] = (\dots, \ln[c], \dots)$, and $[s] = n_s/\Omega$.

The local detailed balance condition (5) ensures that the (average) entropy production rate, quantifying the average dissipated free energy, is specified by^{15–17,19}

$$\langle \dot{\Sigma} \rangle_t = \sum_{\rho, \mathbf{n}_i} R_\rho(\mathbf{n}_i | [\mathbf{c}]_t) P_t(\mathbf{n}_i) \ln \frac{R_\rho(\mathbf{n}_i | [\mathbf{c}]_t) P_t(\mathbf{n}_i)}{R_{-\rho}(\mathbf{n}_i + \mathbf{S}_{i,\rho} | [\mathbf{c}]_t) P_t(\mathbf{n}_i + \mathbf{S}_{i,\rho})}, \quad (8)$$

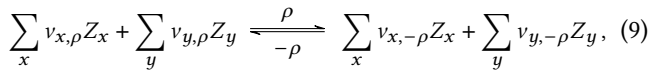
given in units of Boltzmann constant k_B .

III. HYBRID CHEMICAL REACTION NETWORKS

A. Setup

Hybrid CRNs are defined here as closed CRNs where the species $\{i\}$ can be classified, based on their abundances, into *low-abundant* species (labeled x) and *high-abundant* species (labeled y). In a large volume $\Omega \rightarrow \infty$, the low-abundant species have finite molecule numbers n_x , while the high-abundant species have finite concentrations, defined as $[y] \equiv n_y/\Omega$.

In this framework, the chemical equation (1) specializes to



and the set of reactions \mathcal{R} can be split into *continuous* \mathcal{R}_c and *discrete* \mathcal{R}_d reactions. Each reaction ρ is a continuous reaction if it does not affect the abundance of the low-abundant species.³³ Namely,

$$\mathcal{R}_c \equiv \{\rho \in \mathcal{R} \mid \mathbf{S}_{x,\rho} = \mathbf{0}\}, \quad (10)$$

while $\mathbf{S}_{y,\rho} \neq \mathbf{0} \forall \rho \in \mathcal{R}_c$. In contrast, the discrete reactions

$$\mathcal{R}_d \equiv \mathcal{R} \setminus \mathcal{R}_c. \quad (11)$$

affect the abundance of the low-abundant species.³³ Namely, $\mathbf{S}_{x,\rho} \neq \mathbf{0} \forall \rho \in \mathcal{R}_d$. The terms continuous and discrete reactions are chosen anticipating the dynamics that they will lead to for the high-abundant and low-abundant species, respectively, in hybrid CRNs (see Subs. III B).

B. Dynamics

The hybrid dynamics is derived (as summarized in Appendix A) by using a systematic perturbation analysis in the limit $\Omega \rightarrow \infty$ of the CME (3) with finite molecule numbers \mathbf{n}_x and finite concentrations $[\mathbf{y}] \equiv (\dots, [y], \dots)$, called *partial*

macroscopic limit.^{33,37} The procedure leads to a closed dynamical description only under the assumption that the (scaled) reaction rates

$$r_\rho(\mathbf{n}_x, [\mathbf{y}]) \equiv \begin{cases} R_\rho(\mathbf{n}_x, \Omega[\mathbf{y}])/\Omega, & \rho \in \mathcal{R}_c \\ R_\rho(\mathbf{n}_x, \Omega[\mathbf{y}]), & \rho \in \mathcal{R}_d \end{cases} \quad (12)$$

with $R_\rho(\mathbf{n}_x, \mathbf{n}_y) \equiv R_\rho(\mathbf{n}_i) |_{\mathbf{n}_i=(\mathbf{n}_x, \mathbf{n}_y)}$ and $\mathbf{n}_y = \Omega[\mathbf{y}]$, satisfy

$$r_\rho(\mathbf{n}_x, [\mathbf{y}]) = \mathcal{O}(1) \text{ for } \Omega \rightarrow \infty. \quad (13)$$

Note that the physical meaning of the scaling in Eq. (13) will become clear at the end of this section.

The resulting dynamics for the concentrations of high-abundant species is, to leading order, a piecewise deterministic process described by the following reaction rate equation (RRE),

$$\partial_t [\mathbf{y} | \mathbf{n}_x]_t = \sum_{\rho \in \mathcal{R}_c} \mathbf{S}_{y,\rho} r_\rho(\mathbf{n}_x, [\mathbf{y} | \mathbf{n}_x]_t), \quad (14)$$

where $[\mathbf{y} | \mathbf{n}_x]_t$ is the vector of the concentrations of the high-abundant species at time t , given the molecule numbers \mathbf{n}_x of the low-abundant species. Physically, the RRE (14) determines a *continuous* evolution of the concentrations of the high-abundant species depending on the low-abundant species. For this reason, the \mathcal{R}_c reactions are called continuous reactions. On the other hand, the resulting dynamics for the molecule numbers of the low-abundant species is, to leading order, a jump process described by the following CME

$$\begin{aligned} \partial_t p_t(\mathbf{n}_x) = & \sum_{\rho \in \mathcal{R}_d} \{r_\rho(\mathbf{n}_x - \mathbf{S}_{x,\rho}, [\mathbf{y} | \mathbf{n}_x - \mathbf{S}_{x,\rho}]_t) p_t(\mathbf{n}_x - \mathbf{S}_{x,\rho}) \\ & - r_\rho(\mathbf{n}_x, [\mathbf{y} | \mathbf{n}_x]_t) p_t(\mathbf{n}_x)\}. \end{aligned} \quad (15)$$

Physically, the CME (15) determines a *discrete* variations of the molecule numbers of the low-abundant species depending on the high-abundant species. For this reason, the \mathcal{R}_d reactions are called discrete reactions. Note that $p_t(\mathbf{n}_x)$ is the leading order approximation of the marginalized joint probability distribution $P_t(\mathbf{n}_x, \mathbf{n}_y)$, i.e., $p_t(\mathbf{n}_x) \simeq \sum_{\mathbf{n}_y} P_t(\mathbf{n}_x, \mathbf{n}_y)$ for $\Omega \rightarrow \infty$ (see Appendix A).

In summary, the molecule numbers \mathbf{n}_x evolve according to a jump process (described by the CME (15)) whose reaction rates depend on the concentrations of the high-abundant species. During the dwell time between one jump and the next one, the concentrations $[\mathbf{y}]$ of the high-abundant species evolve according to a deterministic process (described by RRE (14)) whose rates depend on the molecule number of the low-abundant species. Furthermore, since the reaction rates featuring the CME (15) and the RRE (14) are of the same order because of the scaling condition in Eq. (13), the molecule numbers \mathbf{n}_x and the concentrations $[\mathbf{y}]$ evolve on the same time scale.

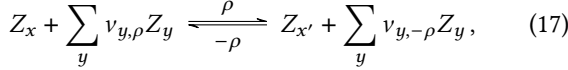
IV. HYBRID DYNAMICS OF ELEMENTARY REACTIONS

A. Mass-action kinetics

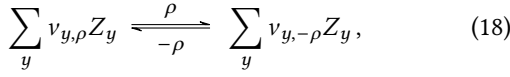
The hybrid dynamics summarized in Subs. III B and App. A is valid for any reaction rates $R_\rho(\mathbf{n}_x, \mathbf{n}_y)$ satisfying the scaling condition in Eq. (13). Here, as well as throughout the paper, we focus on elementary reactions in ideal dilute mixtures satisfying mass-action kinetics, whose reaction rates (4) can be rewritten as

$$R_\rho(\mathbf{n}_x, \mathbf{n}_y) = \Omega k_\rho \prod_x \frac{n_x!}{(n_x - v_{x,\rho})! \Omega^{v_{x,\rho}}} \prod_y \frac{n_y!}{(n_y - v_{y,\rho})! \Omega^{v_{y,\rho}}}, \quad (16)$$

when considering closed CRNs and the splitting of the chemical species into low- and high-abundant ones. Since the volume dependence of the reaction rates in Eq. (16) is determined by the stoichiometric coefficients $\{v_{x,\rho}\}$ and $\{v_{y,\rho}\}$, only specific stoichiometries ensure that the scaling condition in Eq. (13) is satisfied. In particular, by comparing the Ω -dependence in Eq. (16) with Eqs. (12) and (13), we conclude that all discrete reactions must be unimolecular reactions in the low-abundant species, i.e.,



for all $\rho \in \mathcal{R}_d$ and with $x \neq x'$ by definition of discrete reaction. Furthermore, all continuous reactions must not involve the low-abundant species, i.e.,



for all $\rho \in \mathcal{R}_c$. This crucially implies that only hybrid CRNs with discrete and continuous reactions satisfying the stoichiometric conditions in Eqs. (17) and (18) have a well-defined dynamical description (given in Sec. III B) in the partial macroscopic limit.

Remark. If there are no continuous reactions, i.e., $\mathcal{R}_c = \emptyset$, the hybrid dynamics can also be derived when

$$r_\rho(\mathbf{n}_x, [\mathbf{y}]) = R_\rho(\mathbf{n}_x, \Omega[\mathbf{y}]) / \Omega^\alpha, \quad (19)$$

where α is an integer number equal for all $\rho \in \mathcal{R}_d$. Indeed, the scaling condition in Eq. (13) is restored by rescaling time, i.e., by defining $\tau \equiv \Omega^\alpha t$.

B. Emergence of open CRNs with autonomous chemostats

In this section, we prove that the dynamical description of open CRNs with autonomous chemostats emerges from the hybrid dynamics with no continuous reactions. Indeed, in the absence of continuous reactions, the RRE (14) for the high-abundant species boils down to

$$\partial_t [\mathbf{y}]_t = 0, \quad (20)$$

leading to constant concentrations, i.e., $[\mathbf{y}]_t = [\mathbf{y}]_0 \forall t \geq 0$, with $[\mathbf{y}]_0$ being the vector of the initial concentrations of the high-abundant species. By plugging $[\mathbf{y}]_0$ into Eq. (15), the CME for the low-abundant species becomes

$$\partial_t p_t(\mathbf{n}_x) = \sum_{\rho \in \mathcal{R}_d} \{ r_\rho(\mathbf{n}_x - \mathbf{S}_{x,\rho}, [\mathbf{y}]_0) p_t(\mathbf{n}_x - \mathbf{S}_{x,\rho}) - r_\rho(\mathbf{n}_x, [\mathbf{y}]_0) p_t(\mathbf{n}_x) \}, \quad (21)$$

where the reaction rates are given, to leading order, by

$$r_\rho(\mathbf{n}_x, [\mathbf{y}]_0) \simeq \underbrace{\Omega k_\rho \prod_x \frac{n_x!}{(n_x - v_{x,\rho})! \Omega^{v_{x,\rho}}} \prod_y [y]_0^{v_{y,\rho}}}_{=R_\rho(\mathbf{n}_x | [\mathbf{y}]_0)}, \quad (22)$$

with $v_{x,\rho} \neq 0$ only for one specific species according to the stoichiometric conditions in Eq. (17). By now mapping the molecule number \mathbf{n}_x and the concentrations $[\mathbf{y}]_0$ into the molecule number of the internal species \mathbf{n}_i and the concentrations of chemostats $[\mathbf{c}]$ of open CRNs, respectively, the CME (21) of hybrid CRNs becomes equivalent to the CME (3) of open CRNs with autonomous chemostats. This physically means that, to leading order, the hybrid dynamics describes the dynamics of open CRNs with the low- and high-abundant species playing the role of the internal species and autonomous chemostats, respectively.

C. Emergence of open CRNs with evolving chemostats

In this section, we prove that the dynamical description of open CRNs with evolving chemostats emerges from the hybrid dynamics with continuous reactions. Indeed, in the presence of continuous reactions satisfying the stoichiometric conditions in Eq. (18), the RRE (14) for the high-abundant species becomes

$$\partial_t [\mathbf{y}]_t = \sum_{\rho \in \mathcal{R}_c} \mathbf{S}_{y,\rho} r_\rho([\mathbf{y}]_t), \quad (23)$$

with the reaction rates given, to leading order, by

$$r_\rho([\mathbf{y}]_t) \simeq k_\rho \prod_y [y]_t^{v_{y,\rho}} = R_\rho([\mathbf{y}]_t) / \Omega. \quad (24)$$

This implies that the evolution of the concentrations $[\mathbf{y}]_t$ is independent of the low-abundant species (unlike the general RRE (14) which does not account for the constraints resulting from mass-action kinetics). By plugging $[\mathbf{y}]_t$ into Eq. (15), the CME for the low-abundant species becomes

$$\partial_t p_t(\mathbf{n}_x) = \sum_{\rho \in \mathcal{R}_d} \{ r_\rho(\mathbf{n}_x - \mathbf{S}_{x,\rho}, [\mathbf{y}]_t) p_t(\mathbf{n}_x - \mathbf{S}_{x,\rho}) - r_\rho(\mathbf{n}_x, [\mathbf{y}]_t) p_t(\mathbf{n}_x) \}, \quad (25)$$

where the reaction rates are given, to leading order, by

$$r_\rho(\mathbf{n}_x, [\mathbf{y}]_t) \simeq \underbrace{\Omega k_\rho \prod_x \frac{n_x!}{(n_x - v_{x,\rho})! \Omega^{v_{x,\rho}}} \prod_y [y]_t^{v_{y,\rho}}}_{=R_\rho(\mathbf{n}_x | [\mathbf{y}]_t)}, \quad (26)$$

with $v_{x,\rho} \neq 0$ only for one specific species according to the stoichiometric conditions in Eq. (17). By now mapping again the molecule number \mathbf{n}_x and the concentrations $[\mathbf{y}]$ into the molecule number of the internal species \mathbf{n}_i and the concentrations of chemostats $[\mathbf{c}]_t$ of open CRNs, respectively, the CME (25) of hybrid CRNs becomes equivalent to the CME (3) of open CRNs with evolving chemostats. This physically means that, to leading order, the hybrid dynamics describes the dynamics of open CRNs with the low- and high-abundant species playing the role of the internal species and evolving chemostats, respectively. Furthermore, the continuous reactions act as the external processes controlling the concentrations of the chemostats.

V. HYBRID THERMODYNAMICS OF ELEMENTARY REACTIONS

A. Local detailed balance condition

We prove here that the dynamics of hybrid CRNs (Subs. III B) is thermodynamically consistent, namely, it satisfies a local detailed balance condition in the partial macroscopic limit. To do so, we rewrite the general local detailed balance condition in Eq. (5) for closed CRNs where the chemical species are split into low- and high-abundant species,

$$\ln \frac{R_\rho(\mathbf{n}_x, \mathbf{n}_y)}{R_{-\rho}(\mathbf{n}_x + \mathbf{S}_{x,\rho}, \mathbf{n}_y + \mathbf{S}_{y,\rho})} = -\{\Delta_\rho g(\mathbf{n}_x) + \Delta_\rho g(\mathbf{n}_y)\}. \quad (27)$$

We now take the partial macroscopic limit of Eq. (27). By using Eq. (12) together with Eq. (22) or Eq. (26) (depending on whether continuous reactions are present or not) on the left-hand side of Eq. (27), we obtain

$$\ln \frac{R_\rho(\mathbf{n}_x, \mathbf{n}_y)}{R_{-\rho}(\mathbf{n}_x + \mathbf{S}_{x,\rho}, \mathbf{n}_y + \mathbf{S}_{y,\rho})} \simeq \ln \frac{R_\rho(\mathbf{n}_x | [\mathbf{y}])}{R_{-\rho}(\mathbf{n}_x + \mathbf{S}_{x,\rho} | [\mathbf{y}])}, \quad (28)$$

to leading order. Equation (28) boils down to

$$\ln \frac{R_\rho(\mathbf{n}_y)}{R_{-\rho}(\mathbf{n}_y + \mathbf{S}_{y,\rho})} \simeq \ln \frac{R_\rho([\mathbf{y}])}{R_{-\rho}([\mathbf{y}])}, \quad (29)$$

when considering continuous reactions $\rho \in \mathcal{R}_c$, where $v_{x,\rho} = v_{x,-\rho} = 0 \forall x$ because of the stoichiometric conditions in Eq. (18).

We now take the partial macroscopic limit of the right-hand side of Eq. (27). This corresponds to taking the macroscopic limit of the variation of the Gibbs free energy along reaction ρ due to each high-abundant species, i.e., $\Delta_\rho g(\mathbf{n}_y)$. We thus obtain

$$\begin{aligned} \Delta_\rho g(\mathbf{n}_y) &= (\mu_y^\circ - \ln n_s) S_{y,\rho} + \ln(n_y + S_{y,\rho})! - \ln n_y! \\ &\simeq (\mu_y^\circ - \ln n_s) S_{y,\rho} + (u \ln u - u) \Big|_{\Omega[\mathbf{y}]}^{\Omega[\mathbf{y}] + S_{y,\rho}} \\ &\simeq (\mu_y^\circ - \ln n_s) S_{y,\rho} + \ln(\Omega[\mathbf{y}]) S_{y,\rho} \\ &= (\mu_y^\circ + \ln([\mathbf{y}]/[s])) S_{y,\rho} \equiv \mu([\mathbf{y}]) S_{y,\rho}, \end{aligned} \quad (30)$$

by using Stirling's formula, i.e., $\ln n_y! \approx n_y \ln n_y - n_y$, a Taylor expansion for $S_{y,\rho}/(\Omega[\mathbf{y}]) \ll 1$, and by identifying the chemical potential of the high-abundant species as $\mu([\mathbf{y}]) \equiv \mu_y^\circ + \ln([\mathbf{y}]/[s])$.

Finally, by plugging Eqs. (28) and (30) into Eq. (27), we arrive at the following local detailed balance condition

$$\ln \frac{R_\rho(\mathbf{n}_x | [\mathbf{y}])}{R_{-\rho}(\mathbf{n}_x + \mathbf{S}_{x,\rho} | [\mathbf{y}])} = -[\Delta_\rho g(\mathbf{n}_x) + \mu([\mathbf{y}]) \cdot \mathbf{S}_{y,\rho}], \quad (31)$$

which boils down to

$$\ln \frac{R_\rho([\mathbf{y}])}{R_{-\rho}([\mathbf{y}])} = -\mu([\mathbf{y}]) \cdot \mathbf{S}_{y,\rho}, \quad (32)$$

for continuous reactions $\rho \in \mathcal{R}_c$. In practice, the local detailed balance condition (27) of hybrid CRNs converges, in the partial macroscopic limit, to the local detailed balance condition (5) of open CRNs with the low- and high-abundant species playing the role of internal species and chemostats, respectively.

B. Entropy production rate

We derive here the entropy production rate for hybrid CRNs. To do so, we take the partial macroscopic limit of the entropy production rate in Eq. (8), which can be rewritten as

$$\begin{aligned} \langle \dot{\Sigma} \rangle_t &= \sum_{\rho, \mathbf{n}_x, \mathbf{n}_y} R_\rho(\mathbf{n}_x, \mathbf{n}_y) P_t(\mathbf{n}_x, \mathbf{n}_y) \\ &\times \ln \frac{R_\rho(\mathbf{n}_x, \mathbf{n}_y) P_t(\mathbf{n}_x, \mathbf{n}_y)}{R_{-\rho}(\mathbf{n}_x + \mathbf{S}_{x,\rho}, \mathbf{n}_y + \mathbf{S}_{y,\rho}) P_t(\mathbf{n}_x + \mathbf{S}_{x,\rho}, \mathbf{n}_y + \mathbf{S}_{y,\rho})}, \end{aligned} \quad (33)$$

when considering closed CRNs and the splitting of the chemical species into low- and high-abundant ones. Furthermore, like in Sec. III, we consider separately hybrid CRNs with only discrete reactions and hybrid CRNs with also continuous reactions.

1. Hybrid CRNs without continuous reactions

From a dynamical standpoint, in hybrid CRNs without continuous reactions the concentrations $[\mathbf{y}]$ of the high-abundant species are constant in time, i.e., $[\mathbf{y}]_t = [\mathbf{y}]_0 \forall t \geq 0$, and play the role of autonomous chemostats (see Subs. IV B). From a thermodynamic standpoint, only the discrete reactions dissipate and, by taking the partial macroscopic limit of Eq. (33) as formally done in App. B, the entropy production rate converges, to leading order, to

$$\begin{aligned} \langle \dot{\Sigma} \rangle_t &\simeq \sum_{\rho \in \mathcal{R}_d, \mathbf{n}_x} R_\rho(\mathbf{n}_x | [\mathbf{y}]_0) p_t(\mathbf{n}_x) \\ &\times \ln \frac{R_\rho(\mathbf{n}_x | [\mathbf{y}]_0) p_t(\mathbf{n}_x)}{R_{-\rho}(\mathbf{n}_x + \mathbf{S}_{x,\rho} | [\mathbf{y}]_0) p_t(\mathbf{n}_x + \mathbf{S}_{x,\rho})}. \end{aligned} \quad (34)$$

The entropy production rate (34) of hybrid CRNs without continuous reactions is equivalent to the entropy production

rate (8) of open CRNs with autonomous chemostats with the low- and high-abundant species playing the role of the internal species and autonomous chemostats, respectively. Hence, the mapping between hybrid CRNs and open CRNs holds at the dynamical level as well as at the thermodynamic one.

2. Hybrid CRNs with continuous reactions

From a dynamical standpoint, in hybrid CRNs with continuous reactions the concentrations $[\mathbf{y}]_t$ of the high-abundant species evolve in time according to the RRE (23) and play the role of evolving chemostats (see Subs. IV C). From a thermodynamic standpoint, the entropy production rate can be written as the sum of two contributions according to

$$\langle \dot{\Sigma} \rangle_t = \langle \dot{\Sigma}_d \rangle_t + \langle \dot{\Sigma}_c \rangle_t. \quad (35)$$

where $\langle \dot{\Sigma}_d \rangle_t$ and $\langle \dot{\Sigma}_c \rangle_t$ are the entropy production rate of the discrete and continuous reactions, respectively. By now taking the partial macroscopic limit of $\langle \dot{\Sigma}_d \rangle_t$ and $\langle \dot{\Sigma}_c \rangle_t$ as formally done in App. B, we obtain, to leading order,

$$\begin{aligned} \langle \dot{\Sigma}_d \rangle_t &\simeq \sum_{\rho \in \mathcal{R}_d, \mathbf{n}_x} R_\rho(\mathbf{n}_x | [\mathbf{y}]_t) p_t(\mathbf{n}_x) \\ &\times \ln \frac{R_\rho(\mathbf{n}_x | [\mathbf{y}]_t) p_t(\mathbf{n}_x)}{R_{-\rho}(\mathbf{n}_x + \mathbf{S}_{x,\rho} | [\mathbf{y}]_t) p_t(\mathbf{n}_x + \mathbf{S}_{x,\rho})}, \end{aligned} \quad (36)$$

for the discrete reactions and

$$\langle \dot{\Sigma}_c \rangle_t \simeq \sum_{\rho \in \mathcal{R}_c} R_\rho([\mathbf{y}]_t) \ln \frac{R_\rho([\mathbf{y}]_t)}{R_{-\rho}([\mathbf{y}]_t)}, \quad (37)$$

for the continuous reactions.

Let us now examine the meaning of the two expressions in Eqs. (36) and (37). On the one hand, as in Subs. VB 1, the entropy production rate (36) is equivalent to the entropy production rate (8) of open CRNs with evolving chemostats and the mapping between hybrid CRNs and open CRNs holds at the dynamical level as well as at the thermodynamic one. On the other hand, the entropy production rate (37) accounts for the dissipation of the reactions controlling the evolution of the continuous species. Since these reactions play the role of the external processes controlling the chemostats when mapping hybrid CRNs into open CRNs, the entropy production $\langle \dot{\Sigma}_c \rangle_t$ thus quantifies the dissipation of the external processes (which is never accounted for in standard modeling of open CRNs).

We furthermore stress that $\langle \dot{\Sigma}_d \rangle_t$ and $\langle \dot{\Sigma}_c \rangle_t$ are of different order in Ω . The former is Ω -independent since, according to the stoichiometric conditions in Eq. (17), the discrete reactions are unimolecular in the low-abundant species and, therefore, $R_\rho(\mathbf{n}_x | [\mathbf{y}]_t) = \mathcal{O}(1)$ (see mass-action kinetics in Eq. (4)). The latter scales linearly in Ω since, according to the stoichiometric conditions in Eq. (18), the continuous reactions do not involve low-abundant species and, therefore, $R_\rho([\mathbf{y}]_t) = \mathcal{O}(\Omega)$ (see mass-action kinetics in Eq. (4)). Hence,

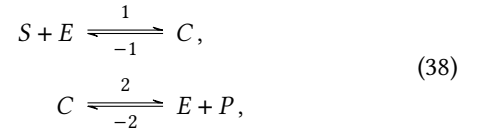
as long as both discrete and continuous reactions do not equilibrate, the entropy production rate of the continuous reactions dominates the entropy production rate of the discrete reactions.

VI. ILLUSTRATIVE EXAMPLES

We now compare the exact dynamics and thermodynamics of closed CRNs with the corresponding hybrid descriptions in the partial macroscopic limit for two prototypical examples.

A. Michaelis-Menten

We consider the Michaelis-Menten CRN



representing the interconversion of a substrate S into a product P catalyzed by the enzyme E via an intermediate complex C . According to mass-action kinetics, the reaction rates of the Michaelis-Menten CRN read

$$R_1(n_E, n_S) = k_1 n_E n_S / \Omega, \quad (39a)$$

$$R_{-1}(n_C) = k_{-1} n_C, \quad (39b)$$

$$R_2(n_C) = k_2 n_C, \quad (39c)$$

$$R_{-2}(n_E, n_P) = k_{-2} n_E n_P / \Omega. \quad (39d)$$

We focus here on the case where substrate and product are high-abundant species, $[\mathbf{y}] \equiv ([S], [P])$, while enzyme and complex are low-abundant species, $\mathbf{n}_x \equiv (n_E, n_C)$. The corresponding hybrid Michaelis-Menten CRN has only discrete reactions, i.e., none of the reactions in Eq. (38) interconverts directly the high-abundant species, namely, substrate and product, without interconverting the low-abundant species, namely, enzyme and complex. The corresponding reaction rates (39) satisfy the scaling condition in Eq. (13) and, to leading order of the partial macroscopic limit, converge to

$$r_1(n_E, [S]) \simeq R_1(n_E | [S]_0) = k_1 n_E [S]_0, \quad (40a)$$

$$r_{-1}(n_C) = R_{-1}(n_C) = k_{-1} n_C, \quad (40b)$$

$$r_2(n_C) = R_2(n_C) = k_2 n_C, \quad (40c)$$

$$r_{-2}(n_E, [P]) \simeq R_{-2}(n_E | [P]_0) = k_{-2} n_E [P]_0, \quad (40d)$$

where $[S]_0$ and $[P]_0$ denote the initial concentration of the substrate and product, which do not evolve in time in the hybrid description since there are no continuous reactions.

We now compare the dynamics and thermodynamics of the closed and hybrid Michaelis-Menten CRNs for different volumes Ω , but with the same concentrations ($[S]_0, [P]_0$) and total molecular number $n_E + n_C$. To do so, we numerically solve the CMEs (3) and (15) with the reaction rates in Eq. (39) and (40), respectively.

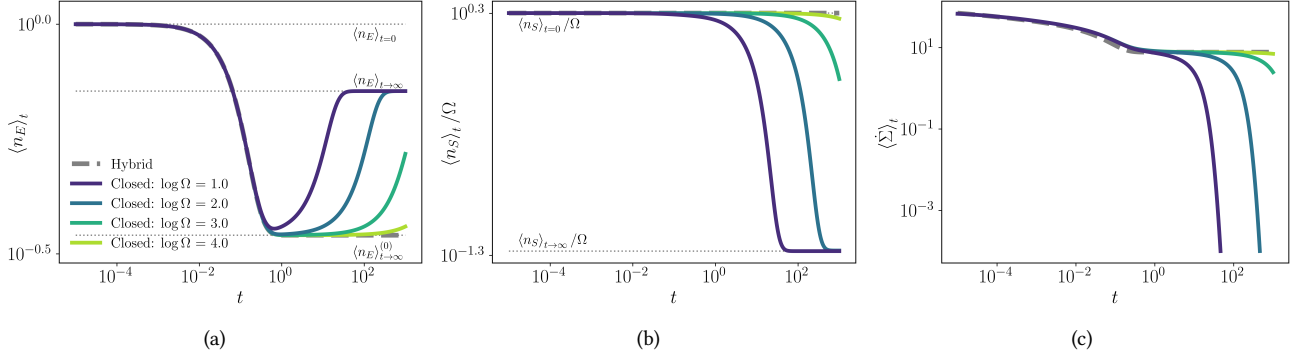


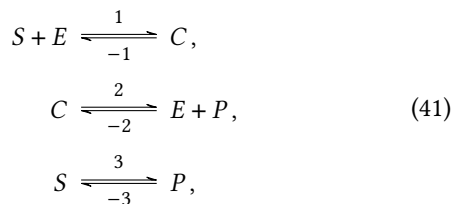
FIG. 1. Dynamics and thermodynamics of the Michaelis-Menten CRN (38). (a) Mean molecule number of the enzyme E (with $\langle n_E \rangle_{t=0}$, $\langle n_E \rangle_{t \rightarrow \infty}$, and $\langle n_E \rangle_{t \rightarrow \infty}^{(0)}$ denoting its initial value, its long-time value resulting from the CME (3) for the closed Michaelis-Menten CRN, and its long-time value resulting from the CME (15) for the hybrid Michaelis-Menten CRN, respectively). (b) Mean concentration of the substrate S (with $\langle n_S \rangle_{t=0}$ and $\langle n_S \rangle_{t \rightarrow \infty}$ denoting the initial mean molecule number and its long-time value resulting from the CME (3) for the closed Michaelis-Menten CRN, respectively). (c) Mean entropy production rate $\langle \dot{\Sigma} \rangle_t$. The initial distribution of the closed Michaelis-Menten CRN is $P_{t=0}(n_E, n_C, n_S, n_P) = \delta(n_E - 1)\delta(n_C)\delta(n_S - [S]_0\Omega)\delta(n_P - [P]_0\Omega)$, the initial distribution of the hybrid Michaelis-Menten CRN is $p_{t=0}(n_E, n_C) = \delta(n_E - 1)\delta(n_C)$, with the initial concentrations (in arbitrary units) $[S]_0 = 2$ and $[P]_0 = 1$. The rate constants are (in arbitrary units) $k_{+1} = k_{+2} = 1/k_{-1} = 1/k_{-2} = e$.

The dynamics of the closed Michaelis-Menten CRN and the hybrid one converge on short time scales. Figure 1a shows the convergence of the mean molecule number of the enzyme $\langle n_E \rangle_t$, while Fig. 1b shows the convergence of the mean concentration of the substrate $\langle n_S \rangle_t / \Omega$ of the closed Michaelis-Menten CRN to the constant concentration $[S]_0$ of the hybrid Michaelis-Menten CRN. By increasing the volume Ω , the convergence between the two descriptions holds for longer time scales, but always fails in the long time limit since the hybrid description does not capture the evolution of the high-abundant species (which play the role of autonomous chemostats). Note that the non-monotonic behavior of $\langle n_E \rangle_t$ is just a consequence of the specific initial conditions used in this case (as already discussed in, for instance, Ref. 48).

The same behavior is observed at the thermodynamic level too. Figure 1c shows that the mean entropy production rates $\langle \dot{\Sigma} \rangle_t$ computed with the two descriptions converge on short time scales (which can be increased by increasing the volume Ω) and diverge in the long time limit. Indeed, the closed Michaelis-Menten CRN relaxes eventually to equilibrium characterized by $\langle \dot{\Sigma} \rangle_t = 0$, while the hybrid Michaelis-Menten CRN stays out of equilibrium because of the high-abundant species acting as autonomous chemostats.

B. Cyclic Michaelis-Menten

We consider the cyclic Michaelis-Menten CRN²⁵



where the reactions ± 1 and ± 2 are the same catalytic reactions of Eq. (38), while reactions ± 3 represent the direct interconversion of the substrate into the product. According to mass-action kinetics, the rates of reactions ± 1 and ± 2 are given in Eq. (39), while the rates of reactions ± 3 read

$$R_3(n_S) = k_3 n_S, \tag{42a}$$

$$R_{-3}(n_P) = k_{-3} n_P. \tag{42b}$$

Note that thermodynamic consistency, i.e., the local detailed balance condition (5), imposes that the kinetic constants of the reactions in Eq. (41) satisfy

$$\frac{k_1 k_2 k_{-3}}{k_{-1} k_{-2} k_3} = 1. \tag{43}$$

This condition, also known as Wegscheider's condition,⁴⁹ ensures that the closed cyclic Michaelis-Menten CRN equilibrates.

As in Subs. VI A, we focus here on the case where substrate and product are high-abundant species. In the corresponding hybrid description, reactions ± 3 are continuous reactions determining the evolution of the concentrations $[\mathbf{y}]_t = ([S]_t, [P]_t)$ according to Eq. (23) with the rates given, to leading order of the partial macroscopic limit, by

$$r_3([S]_t) \simeq R_3([S]_t)/\Omega = k_3 [S]_t, \tag{44a}$$

$$r_{-3}([P]_t) \simeq R_{-3}([P]_t)/\Omega = k_{-3} [P]_t. \tag{44b}$$

The resulting dynamics for $([S]_t, [P]_t)$ can be analytically determined and reads

$$[S]_t = [S]_0 e^{-(k_3 + k_{-3})t} + \frac{k_{-3}([S]_0 + [P]_0)}{k_3 + k_{-3}} \left(1 - e^{-(k_3 + k_{-3})t}\right) \tag{45}$$

and $[P]_t = ([S]_0 + [P]_0) - [S]_t$.

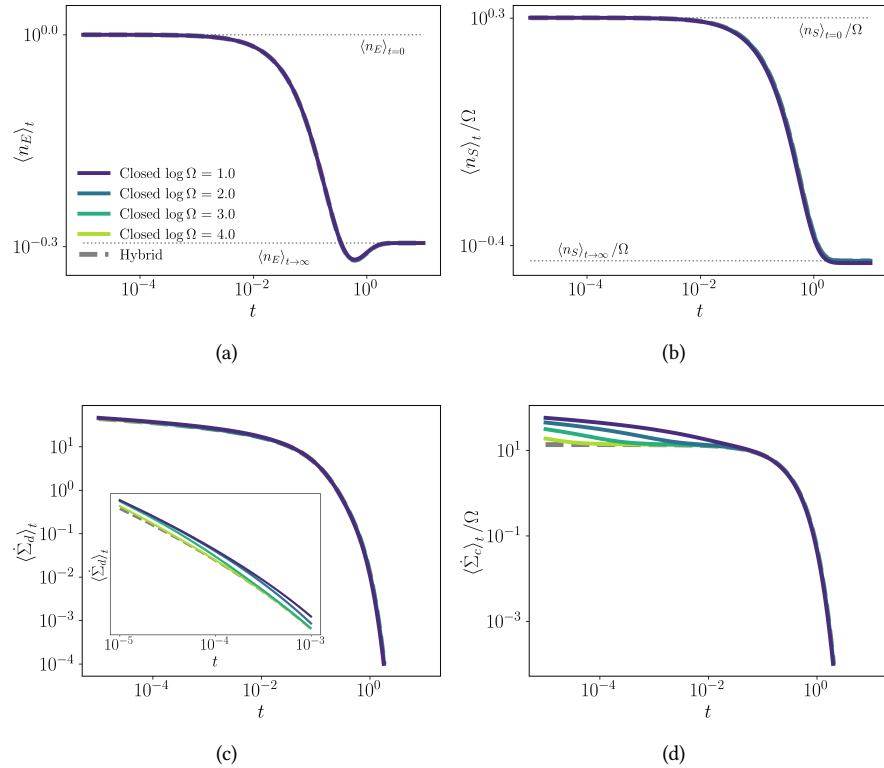


FIG. 2. Dynamics and thermodynamics of the cyclic Michaelis-Menten CRN (41). (a) Mean molecule number of the enzyme E (with $\langle n_E \rangle_{t=0}$ and $\langle n_E \rangle_{t \rightarrow \infty}$, denoting its initial value and its long-time value resulting from the CME (3) for the closed cyclic Michaelis-Menten CRN, respectively). (b) Mean concentration of the substrate S (with $\langle n_S \rangle_{t=0}$ and $\langle n_S \rangle_{t \rightarrow \infty}$ denoting the initial mean molecule number and its long-time value resulting from the CME (3) for the closed cyclic Michaelis-Menten CRN, respectively). (c) Mean entropy production rate of the discrete reactions $\langle \dot{\Sigma}_d \rangle_t$. (d) Mean entropy production rate of the continuous reaction $\langle \dot{\Sigma}_c \rangle_t$. The initial distribution of the closed cyclic Michaelis-Menten CRN is $P_{t=0}(n_E, n_C, n_S, n_P) = \delta(n_E - 1)\delta(n_C)\delta(n_S - [S]_0\Omega)\delta(n_P - [P]_0\Omega)$, the initial distribution of the hybrid cyclic Michaelis-Menten CRN is $p_{t=0}(n_E, n_C) = \delta(n_E - 1)\delta(n_C)$, with the initial concentrations (in arbitrary units) $[S]_0 = 2$ and $[P]_0 = 1$. The rate constants are (in arbitrary units) $\log k_1 = \log k_2 = -\log k_{-1} = -\log k_{-2} = 1/2$ and $\log k_3 = -\log k_{-3} = 1$.

Reactions ± 1 and ± 2 are still discrete reactions, whose rates are still given, to leading order, in Eq. (40) once the initial concentrations ($[S]_0, [P]_0$) are replaced by the instantaneous ones ($[S]_t, [P]_t$).

We now compare the dynamics and thermodynamics of the closed and hybrid cyclic Michaelis-Menten CRNs for different volumes Ω , but with the same initial concentrations ($[S]_0, [P]_0$) and total molecular number $n_E + n_C$. To do so, we numerically solve the CMEs (3) and (15) with the concentrations $[\mathbf{y}]_t$ given in Eq. (45).

The dynamics of the closed cyclic Michaelis-Menten CRN and the hybrid one converge on both short and long time scales. Figure 2a shows the convergence of the mean molecule number of the enzyme $\langle n_E \rangle_t$, while Fig. 2b shows the convergence of the mean concentration of the substrate $\langle n_S \rangle_t / \Omega$ of the closed cyclic Michaelis-Menten CRN to the concentration $[S]_t$ of the hybrid cyclic Michaelis-Menten CRN. The convergence on long time scales results from the continuous reaction which ensures that the evolution of the high-abundant species in the hybrid description well reproduces their evolution in the closed cyclic Michaelis-Menten CRN. Note that, like in Fig. 1a, the non-monotonic behavior

of $\langle n_E \rangle_t$ is just a consequence of the specific initial conditions used in this case (as already discussed in, for instance, Ref. 48).

A similar behavior, namely, a convergence of the two descriptions at both short and long time scales, is observed for the mean entropy production rates of the discrete reactions in Fig. 2c. Furthermore, in both descriptions, the CRN relaxes eventually to equilibrium characterized by $\langle \dot{\Sigma}_d \rangle_t = 0$ and, indeed, the mean entropy production rates in Fig. 2c monotonously decrease. On the other hand, the mean entropy production rates of the continuous reaction $\langle \dot{\Sigma}_c \rangle_t$ in Fig. 2d computed with the two descriptions converge on long time scales (where the reaction equilibrates and $\langle \dot{\Sigma}_c \rangle_t = 0$), but do not match on short time scales for small volumes Ω . This is due to the correlations between the low- and high-abundant species in the closed cyclic Michaelis-Menten CRN, which are lost in the hybrid cyclic Michaelis-Menten CRN where the evolution of the high-abundant species is independent of the low-abundant ones. These correlations become less relevant for larger volumes Ω (see Fig. 2d). Note that a similar trend can be observed for the mean entropy production rates of the discrete reactions in the inset in Fig. 2c.

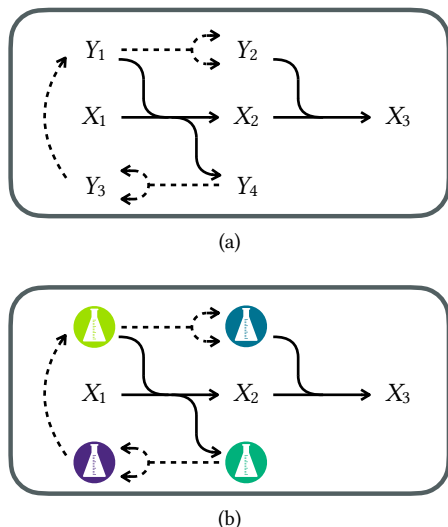


FIG. 3. Exemplary hybrid CRN whose stoichiometry satisfies the scaling conditions in Eq. (13). (a) Closed CRN with low-abundant species (X_1, X_2, X_3) and high-abundant species (Y_1, Y_2, Y_3, Y_4). (b) Open CRN with internal species (X_1, X_2, X_3) and chemostats represented by Erlenmeyer flasks of different colors. In the partial macroscopic limit, the closed CRN (a) converges to the open one (b). Arrows represent the forward chemical reactions using hypergraph notation, while backward reactions are not illustrated for simplicity. Solid arrows represent discrete reactions (Eq. (11)) that are unimolecular in the low-abundant (resp. internal) species, while having arbitrary stoichiometry in the high-abundant species (resp. chemostats). Dashed arrows represent continuous reactions (Eq. (10)) that do not involve low-abundant (resp. internal) species and have arbitrary stoichiometry in the high-abundant species (resp. chemostats).

However, the mismatch for $\langle \dot{\Sigma}_d \rangle_t$ on short time scales is of a smaller magnitude compared to the mismatch for $\langle \dot{\Sigma}_c \rangle_t$ since the discrete reactions depend on the high-abundant species also in the hybrid cyclic Michaelis-Menten CRN and hence keep track of the correlations between the two sets of species.

VII. DISCUSSION & CONCLUSION

In this work, we showed that the dynamics (Sec. IV) and thermodynamics (Sec. V) of open CRNs following mass-action kinetics can emerge from closed CRNs, when specific stoichiometric conditions are satisfied (see Fig. 3). In partic-

ular, open CRNs with unimolecular reactions in the internal species result from the partial macroscopic limit of hybrid CRNs with discrete reactions that are unimolecular in the low-abundant species (see Eq. (17)) and continuous reactions that do not involve the low-abundant species (see Eq. (18)). On the one hand, the low-abundant species and the discrete reactions of hybrid CRNs become the internal species and the reactions of open CRNs, respectively. Correspondingly, the entropy production rate of the discrete reactions quantifies the dissipation of open CRNs. On the other hand, the high-abundant species and the continuous reactions of hybrid CRNs become the chemostats of open CRNs and their driving protocols, respectively. Correspondingly, the entropy production rate of the continuous reactions quantifies the dissipation of the driving protocols, usually neglected in the modeling of open CRNs.

We note that, to the best of our knowledge, only Ref. 50 examined thermodynamic-like observables for hybrid CRNs by establishing a fluctuation relation for the dynamics of the high-abundant species. However, contrary to our work, they built this relation directly on the hybrid dynamics instead of considering how it emerges from the microscopic scale by taking the partial macroscopic limit.

While our work clearly demonstrates how chemostats can result from an underlying closed CRN, it does so for a subset of all possible stoichiometries. This is a direct implication of the large volume limit developed in Refs. 32–38 which is based on a single-scale perturbation analysis. To investigate the emergence of chemostats in CRNs not satisfying the stoichiometric conditions in Eqs. (17) and (18), a multi-scale perturbation analysis needs to be developed and used. We leave this to further studies.

ACKNOWLEDGMENTS

BR and ME are supported by the Fond National de la Recherche-FNR, Luxembourg by the Project ChemComplex (C21/MS/16356329). FA is supported by the project P-DiSC#BIRD2023-UNIPD funded by the Department of Chemical Sciences of the University of Padova (Italy).

DATA AVAILABILITY

The data that support the findings of this study are available from the corresponding author upon reasonable request.

Appendix A: Derivation of the dynamics of hybrid CRNs

We review here the general derivation of the hybrid dynamics in the partial macroscopic limit summarized in Subs. III B by following the original derivation in Ref. 33 (which does not assume that the reaction rates satisfy mass-action kinetics). We

start by rewriting the CME (3) for hybrid CRNs (defined in Subs. III A) as

$$\begin{aligned} \partial_t P_t(\mathbf{n}_x, \mathbf{n}_y) = & \sum_{\rho \in \mathcal{R}_d} \{R_\rho(\mathbf{n}_x - \mathbf{S}_{x,\rho}, \mathbf{n}_y - \mathbf{S}_{y,\rho})P_t(\mathbf{n}_x - \mathbf{S}_{x,\rho}, \mathbf{n}_y - \mathbf{S}_{y,\rho}) - R_\rho(\mathbf{n}_x, \mathbf{n}_y)P_t(\mathbf{n}_x, \mathbf{n}_y)\} \\ & + \sum_{\rho \in \mathcal{R}_c} \{R_\rho(\mathbf{n}_x, \mathbf{n}_y - \mathbf{S}_{y,\rho})P_t(\mathbf{n}_x, \mathbf{n}_y - \mathbf{S}_{y,\rho}) - R_\rho(\mathbf{n}_x, \mathbf{n}_y)P_t(\mathbf{n}_x, \mathbf{n}_y)\}, \end{aligned} \quad (\text{A1})$$

by accounting for the splitting of the chemical species into low-abundant (labeled x) and high-abundant (labeled y) species as well as the splitting of the chemical reactions \mathcal{R} into discrete \mathcal{R}_d and continuous \mathcal{R}_c reactions. We then take the partial macroscopic limit, namely, the large volume limit $\Omega \rightarrow \infty$ characterized by finite molecule numbers \mathbf{n}_x and finite concentrations $[\mathbf{y}] \equiv (\dots, [y], \dots)$, of the CME (A1). To do so, we need to consider how the reaction rates $\{R_\rho(\mathbf{n}_x, \mathbf{n}_y)\}$ and the probability $P_t(\mathbf{n}_x, \mathbf{n}_y)$ depend on Ω .

First, we consider the reaction rates $\{R_\rho(\mathbf{n}_x, \mathbf{n}_y)\}$. By assuming the scaling conditions in Eqs. (12) and (13), the CME (A1) becomes

$$\begin{aligned} \partial_t P_t(\mathbf{n}_x, \mathbf{n}_y) = & \sum_{\rho \in \mathcal{R}_d} \left\{ r_\rho \left(\mathbf{n}_x - \mathbf{S}_{x,\rho}, [\mathbf{y}] - \frac{\mathbf{S}_{y,\rho}}{\Omega} \right) P_t(\mathbf{n}_x - \mathbf{S}_{x,\rho}, \mathbf{n}_y - \mathbf{S}_{y,\rho}) - r_\rho(\mathbf{n}_x, [\mathbf{y}]) P_t(\mathbf{n}_x, \mathbf{n}_y) \right\} \\ & + \Omega \sum_{\rho \in \mathcal{R}_c} \left\{ r_\rho \left(\mathbf{n}_x, [\mathbf{y}] - \frac{\mathbf{S}_{y,\rho}}{\Omega} \right) P_t(\mathbf{n}_x, \mathbf{n}_y - \mathbf{S}_{y,\rho}) - r_\rho(\mathbf{n}_x, [\mathbf{y}]) P_t(\mathbf{n}_x, \mathbf{n}_y) \right\}, \end{aligned} \quad (\text{A2})$$

with $r_\rho(\mathbf{n}_x, [\mathbf{y}]) = \mathcal{O}(1)$ for $\Omega \rightarrow \infty$.

Second, we consider the probability $P_t(\mathbf{n}_x, \mathbf{n}_y)$. We rewrite it as

$$P_t(\mathbf{n}_x, \mathbf{n}_y) = P_t(\mathbf{n}_y | \mathbf{n}_x) P_t(\mathbf{n}_x), \quad (\text{A3})$$

and use the change of variables from \mathbf{n}_y to $[\mathbf{y}]$ to define

$$p_t^{(\Omega)}([\mathbf{y}] | \mathbf{n}_x) p_t^{(\Omega)}(\mathbf{n}_x) \equiv \Omega^{N_y} P_t(\Omega[\mathbf{y}] | \mathbf{n}_x) P_t(\mathbf{n}_x), \quad (\text{A4})$$

where N_y denotes the total number of high-abundant species and the superscript Ω highlights that the probabilities on the left-hand side of Eq. (A4) depend on the volume. In the partial macroscopic limit, we use the Wentzel–Kramers–Brillouin (WKB) ansatz^{39–44} for the conditional probability distribution $p_t^{(\Omega)}([\mathbf{y}] | \mathbf{n}_x)$:

$$p_t^{(\Omega)}([\mathbf{y}] | \mathbf{n}_x) = C_\Omega e^{-\Omega I_t([\mathbf{y}] | \mathbf{n}_x)} \sum_{k=0}^{\infty} U_t^{(k)}([\mathbf{y}] | \mathbf{n}_x) \Omega^{-k}, \quad (\text{A5})$$

where C_Ω is the normalization constant, $I_t([\mathbf{y}] | \mathbf{n}_x)$ is the zero-order rate function, and each $U_t^{(k)}([\mathbf{y}] | \mathbf{n}_x)$ is a subexponential correction of order Ω^{-k} . Furthermore, we use a perturbation expansion series for the marginalized distribution of the discrete species $p_t^{(\Omega)}(\mathbf{n}_x)$ in powers of $1/\Omega$:

$$p_t^{(\Omega)}(\mathbf{n}_x) = p_t(\mathbf{n}_x) + \sum_{k=1}^{\infty} p_t^{(k)}(\mathbf{n}_x) \Omega^{-k}. \quad (\text{A6})$$

By now using Eqs. (A5) and (A6) in the CME (A2), the leading order $\mathcal{O}(\Omega)$ of its left-hand-side reads

$$-\Omega C_\Omega e^{-\Omega I_t([\mathbf{y}] | \mathbf{n}_x)} U_t^{(0)}([\mathbf{y}] | \mathbf{n}_x) p_t(\mathbf{n}_x) \partial_t I_t([\mathbf{y}] | \mathbf{n}_x), \quad (\text{A7})$$

while the leading order $\mathcal{O}(\Omega)$ of its right-hand-side emerges only from the continuous reactions and reads

$$\Omega C_\Omega e^{-\Omega I_t([\mathbf{y}] | \mathbf{n}_x)} U_t^{(0)}([\mathbf{y}] | \mathbf{n}_x) p_t(\mathbf{n}_x) \sum_{\rho \in \mathcal{R}_c} r_\rho(\mathbf{n}_x, [\mathbf{y}]) \left\{ e^{\nabla_{[\mathbf{y}]} I_t([\mathbf{y}] | \mathbf{n}_x) \cdot \mathbf{S}_{y,\rho}} - 1 \right\}, \quad (\text{A8})$$

with $\nabla_{[\mathbf{y}]} = (\dots, \partial_{[y]}, \dots)$. Hence, the leading order $\mathcal{O}(\Omega)$ of the CME (A2) reads

$$\partial_t I_t([\mathbf{y}] | \mathbf{n}_x) = - \sum_{\rho \in \mathcal{R}_c} r_\rho(\mathbf{n}_x, [\mathbf{y}]) \left\{ e^{\nabla_{[\mathbf{y}]} I_t([\mathbf{y}] | \mathbf{n}_x) \cdot \mathbf{S}_{y,\rho}} - 1 \right\} \equiv -H([\mathbf{y}], \nabla_{[\mathbf{y}]} I_t([\mathbf{y}] | \mathbf{n}_x) | \mathbf{n}_x), \quad (\text{A9})$$

where we introduced the Hamiltonian $H(\mathbf{q}, \xi | \mathbf{n}_x)$ with the variables \mathbf{q} and the conjugated variables ξ corresponding to $[\mathbf{y}]$ and $\nabla_{[\mathbf{y}]} I_t([\mathbf{y}] | \mathbf{n}_x)$, respectively.

Finally, we assume that the conditional probability distribution $p_t^{(\Omega)}([\mathbf{y}] | \mathbf{n}_x)$ has a unique maximum at every time t , denoted $[\mathbf{y} | \mathbf{n}_x]_t$, with the necessary condition for its existence given by

$$\xi_t \equiv \nabla_{[\mathbf{y}]} I_t([\mathbf{y}] | \mathbf{n}_x) \Big|_{[\mathbf{y}] = [\mathbf{y} | \mathbf{n}_x]_t} \stackrel{!}{=} \mathbf{0}. \quad (\text{A10})$$

The existence of this maximum leads to the RRE (14) for the concentrations of the high-abundant species and the CME (15) for the low-abundant species. Indeed, $[\mathbf{y} | \mathbf{n}_x]_t$ defines the most probable concentrations of the high-abundant species and evolves in time according to the following Hamilton equation

$$\partial_t [\mathbf{y} | \mathbf{n}_x]_t = \nabla_{\xi} H([\mathbf{y} | \mathbf{n}_x]_t, \xi | \mathbf{n}_x) \Big|_{\xi = \mathbf{0}} = \sum_{\rho \in \mathcal{R}_c} \mathbf{S}_{y,\rho} r_{\rho}(\mathbf{n}_x, [\mathbf{y} | \mathbf{n}_x]_t), \quad (\text{A11})$$

which is RRE (14) in the main text. On the other hand, a CME for the low-abundant species can be obtained by marginalizing the CME (A2),

$$\begin{aligned} \partial_t p_t^{(\Omega)}(\mathbf{n}_x) &= \int d[\mathbf{y}] \partial_t \left\{ p_t^{(\Omega)}([\mathbf{y}] | \mathbf{n}_x) p_t^{(\Omega)}(\mathbf{n}_x) \right\} \\ &= \sum_{\rho \in \mathcal{R}_d} \int d[\mathbf{y}] \left\{ r_{\rho} \left(\mathbf{n}_x - \mathbf{S}_{x,\rho}, [\mathbf{y}] - \frac{\mathbf{S}_{y,\rho}}{\Omega} \right) p_t^{(\Omega)} \left([\mathbf{y}] - \frac{\mathbf{S}_{y,\rho}}{\Omega} \Big| \mathbf{n}_x - \mathbf{S}_{x,\rho} \right) p_t^{(\Omega)}(\mathbf{n}_x - \mathbf{S}_{x,\rho}) \right. \\ &\quad \left. - r_{\rho}(\mathbf{n}_x, [\mathbf{y}]) p_t^{(\Omega)}([\mathbf{y}] | \mathbf{n}_x) p_t^{(\Omega)}(\mathbf{n}_x) \right\}, \end{aligned} \quad (\text{A12})$$

together with Laplace's saddle-node approximation, i.e.,

$$\int d[\mathbf{y}] p_t^{(\Omega)}([\mathbf{y}] | \mathbf{n}_x) f(\mathbf{n}_x, [\mathbf{y}]) = f(\mathbf{n}_x, [\mathbf{y} | \mathbf{n}_x]_t) + \mathcal{O}(\Omega^{-1}). \quad (\text{A13})$$

We, thus, find

$$\partial_t p_t(\mathbf{n}_x) = \sum_{\rho \in \mathcal{R}_d} \left\{ r_{\rho}(\mathbf{n}_x - \mathbf{S}_{x,\rho}, [\mathbf{y} | \mathbf{n}_x - \mathbf{S}_{x,\rho}]_t) p_t(\mathbf{n}_x - \mathbf{S}_{x,\rho}) - r_{\rho}(\mathbf{n}_x, [\mathbf{y} | \mathbf{n}_x]_t) p_t(\mathbf{n}_x) \right\}. \quad (\text{A14})$$

which is CME (15) in the main text.

Appendix B: Derivation of the entropy production rate for hybrid CRNs

We derive here the partial macroscopic limit of the entropy production rate for hybrid CRNs whose reactions satisfy the stoichiometric conditions in Eqs. (17) and (18). We start by rewriting its general expression in Eq. (8) as

$$\begin{aligned} \langle \dot{\Sigma} \rangle_t &= \sum_{\rho \in \mathcal{R}_d} \sum_{\mathbf{n}_x, \mathbf{n}_y} R_{\rho}(\mathbf{n}_x, \mathbf{n}_y) P_t(\mathbf{n}_x, \mathbf{n}_y) \ln \frac{R_{\rho}(\mathbf{n}_x, \mathbf{n}_y) P_t(\mathbf{n}_x, \mathbf{n}_y)}{R_{-\rho}(\mathbf{n}_x + \mathbf{S}_{x,\rho}, \mathbf{n}_y + \mathbf{S}_{y,\rho}) P_t(\mathbf{n}_x + \mathbf{S}_{x,\rho}, \mathbf{n}_y + \mathbf{S}_{y,\rho})} \\ &\quad + \sum_{\rho \in \mathcal{R}_c} \sum_{\mathbf{n}_x, \mathbf{n}_y} R_{\rho}(\mathbf{n}_y) P_t(\mathbf{n}_x, \mathbf{n}_y) \ln \frac{R_{\rho}(\mathbf{n}_y) P_t(\mathbf{n}_x, \mathbf{n}_y)}{R_{-\rho}(\mathbf{n}_y + \mathbf{S}_{y,\rho}) P_t(\mathbf{n}_x, \mathbf{n}_y + \mathbf{S}_{y,\rho})} \end{aligned} \quad (\text{B1})$$

by accounting for the splitting of the chemical species into low-abundant (labeled x) and high-abundant (labeled y) species as well as the splitting of the chemical reactions \mathcal{R} into discrete \mathcal{R}_d and continuous \mathcal{R}_c reactions (where the latter do not depend on the low-abundant species because of stoichiometric conditions in Eq. (18)). We then express the reaction rates in terms of $\{r_{\rho}(\mathbf{n}_x, [\mathbf{y}])\}$ (defined in Eq. (12) and satisfying the scaling condition in Eq. (13)) and the probability $P_t(\mathbf{n}_x, \mathbf{n}_x)$ in terms of $p_t^{(\Omega)}([\mathbf{y}] | \mathbf{n}_x)$ and $p_t^{(\Omega)}(\mathbf{n}_x)$ given in Eq. (A4). We thus obtain

$$\begin{aligned} \langle \dot{\Sigma} \rangle_t &= \sum_{\rho \in \mathcal{R}_d} \sum_{\mathbf{n}_x} \int d[\mathbf{y}] r_{\rho}(\mathbf{n}_x, [\mathbf{y}]) p_t^{(\Omega)}([\mathbf{y}] | \mathbf{n}_x) p_t^{(\Omega)}(\mathbf{n}_x) \ln \frac{r_{\rho}(\mathbf{n}_x, [\mathbf{y}]) p_t^{(\Omega)}([\mathbf{y}] | \mathbf{n}_x) p_t^{(\Omega)}(\mathbf{n}_x)}{r_{-\rho} \left(\mathbf{n}_x + \mathbf{S}_{x,\rho}, [\mathbf{y}] + \frac{\mathbf{S}_{y,\rho}}{\Omega} \right) p_t^{(\Omega)} \left([\mathbf{y}] + \frac{\mathbf{S}_{y,\rho}}{\Omega} \Big| \mathbf{n}_x + \mathbf{S}_{x,\rho} \right) p_t^{(\Omega)}(\mathbf{n}_x + \mathbf{S}_{x,\rho})} \\ &\quad + \Omega \sum_{\rho \in \mathcal{R}_c} \sum_{\mathbf{n}_x} p_t^{(\Omega)}(\mathbf{n}_x) \int d[\mathbf{y}] r_{\rho}([\mathbf{y}]) p_t^{(\Omega)}([\mathbf{y}] | \mathbf{n}_x) \ln \frac{r_{\rho}([\mathbf{y}]) p_t^{(\Omega)}([\mathbf{y}] | \mathbf{n}_x)}{r_{-\rho} \left([\mathbf{y}] + \frac{\mathbf{S}_{y,\rho}}{\Omega} \right) p_t^{(\Omega)} \left([\mathbf{y}] + \frac{\mathbf{S}_{y,\rho}}{\Omega} \Big| \mathbf{n}_x \right)}, \end{aligned} \quad (\text{B2})$$

by replacing the sum $\sum_{\mathbf{n}_y}$ with the integral $\int d[\mathbf{y}]$. Finally, by Taylor expanding the small terms $S_{y,\rho}/\Omega$, using Laplace's saddle-node approximation (A13), and recognizing that the leading order contribution of $p_t^{(\Omega)}([\mathbf{y}|\mathbf{n}_x)$ as well as the corresponding maximum $[\mathbf{y}|\mathbf{n}_x]_t$ are \mathbf{n}_x -independent if the continuous reactions do not involve the low-abundant species (see Ref. 33) as imposed by the stoichiometric conditions (18), the entropy production rate becomes, to leading order,

$$\langle \dot{\Sigma} \rangle_t = \underbrace{\sum_{\rho \in \mathcal{R}_d, \mathbf{n}_x} r_\rho(\mathbf{n}_x, [\mathbf{y}]_t) p_t(\mathbf{n}_x) \ln \frac{r_\rho(\mathbf{n}_x, [\mathbf{y}]_t) p_t(\mathbf{n}_x)}{r_{-\rho}(\mathbf{n}_x + \mathbf{S}_{x,\rho}, [\mathbf{y}]_t) p_t(\mathbf{n}_x + \mathbf{S}_{x,\rho})}}_{\simeq \langle \dot{\Sigma}_d \rangle_t} + \Omega \underbrace{\sum_{\rho \in \mathcal{R}_c} r_\rho([\mathbf{y}]_t) \ln \frac{r_\rho([\mathbf{y}]_t)}{r_{-\rho}([\mathbf{y}]_t)}}_{\simeq \langle \dot{\Sigma}_c \rangle_t}, \quad (\text{B3})$$

where we also recognize the entropy production rate of the discrete and continuous reactions. Note that the leading order contributions to the entropy production rate of the discrete and continuous reactions are of order $\mathcal{O}(1)$ and $\mathcal{O}(\Omega)$, respectively. This implies that the next order contribution to $\langle \dot{\Sigma}_c \rangle_t$ is of the same order of $\langle \dot{\Sigma}_d \rangle_t$, i.e., $\mathcal{O}(1)$. This does not constitute an inconsistency of our theory since, as explained in Subs. V B 2, discrete and continuous reactions have different physical meanings. The former represent the chemical reactions of an open CRN, while the latter represent the external processes controlling the chemostats.

- ¹X. Yang, M. Heinemann, J. Howard, G. Huber, S. Iyer-Biswas, G. L. Treut, M. Lynch, K. L. Montooth, D. J. Needleman, S. Pigolotti, J. Rodenfels, P. Ronceray, S. Shankar, I. Tavassoly, S. Thutupalli, D. V. Titov, J. Wang, and P. J. Foster, "Physical bioenergetics: Energy fluxes, budgets, and constraints in cells," *Proc. Natl. Acad. Sci. U.S.A.* **118**, e2026786118 (2021).
- ²G. Ashkenasy, T. M. Hermans, S. Otto, and A. F. Taylor, "Systems chemistry," *Chem. Soc. Rev.* **46**, 2543–2554 (2017).
- ³M. Esposito, "Open questions on nonequilibrium thermodynamics of chemical reaction networks," *Communications Chemistry* **3**, 107 (2020).
- ⁴A. Wachtel, R. Rao, and M. Esposito, "Free-energy transduction in chemical reaction networks: From enzymes to metabolism," *J. Chem. Phys.* **157**, 024109 (2022).
- ⁵M. Bilancioni and M. Esposito, "Gears in chemical reaction networks: Optimizing energy transduction efficiency," (2025), arXiv:2405.17960.
- ⁶D. Voet and J. G. Voet, *Biochemistry* (J. Wiley & Sons, 2010).
- ⁷P. Solís Muñana, G. Ragazzon, J. Dupont, C. Z. J. Ren, L. J. Prins, and J. L. Y. Chen, "Substrate-induced self-assembly of cooperative catalysts," *Angew. Chem. Int. Ed.* **57**, 16469–16474 (2018).
- ⁸K. Das, L. Gabrielli, and L. J. Prins, "Chemically fueled self-assembly in biology and chemistry," *Angew. Chem. Int. Ed.* **60**, 20120–20143 (2021).
- ⁹D. Andrieux and P. Gaspard, "Fluctuation theorem and mesoscopic chemical clocks," *J. Chem. Phys.* **128**, 154506 (2008).
- ¹⁰P. Gaspard, "Stochastic approach to entropy production in chemical chaos," *Chaos* **30**, 113103 (2020).
- ¹¹B. Altaner, A. Wachtel, and J. Vollmer, "Fluctuating currents in stochastic thermodynamics. ii. energy conversion and nonequilibrium response in kinesin models," *Phys. Rev. E* **92**, 042133 (2015).
- ¹²G. Falasco, T. Cossetto, E. Penocchio, and M. Esposito, "Negative differential response in chemical reactions," *New J. Phys.* **21**, 073005 (2019).
- ¹³D. Forastiere, G. Falasco, and M. Esposito, "Strong current response to slow modulation: A metabolic case-study," *J. Chem. Phys.* **152**, 134101 (2020).
- ¹⁴S. G. Marehalli Srinivas, M. Poletti, M. Esposito, and F. Avanzini, "Deficiency, kinetic invertibility, and catalysis in stochastic chemical reaction networks," *J. Chem. Phys.* **158**, 204108 (2023).
- ¹⁵P. Gaspard, "Fluctuation theorem for nonequilibrium reactions," *J. Chem. Phys.* **120**, 8898–8905 (2004).
- ¹⁶T. Schmiedl and U. Seifert, "Stochastic thermodynamics of chemical reaction networks," *J. Chem. Phys.* **126**, 044101 (2007).
- ¹⁷R. Rao and M. Esposito, "Conservation laws and work fluctuation relations in chemical reaction networks," *J. Chem. Phys.* **149**, 245101 (2018).
- ¹⁸H. Qian and D. A. Beard, "Thermodynamics of stoichiometric biochemical networks in living systems far from equilibrium," *Biophys. Chem.* **114**, 213 – 220 (2005).
- ¹⁹R. Rao and M. Esposito, "Nonequilibrium thermodynamics of chemical reaction networks: Wisdom from stochastic thermodynamics," *Phys. Rev. X* **6**, 041064 (2016).
- ²⁰F. Avanzini, E. Penocchio, G. Falasco, and M. Esposito, "Nonequilibrium thermodynamics of non-ideal chemical reaction networks," *J. Chem. Phys.* **154**, 094114 (2021).
- ²¹F. Avanzini, M. Bilancioni, V. Cavina, S. D. Cengio, M. Esposito, G. Falasco, D. Forastiere, N. Freitas, A. Garilli, P. E. Harunari, V. Lecomte, A. Lazarescu, S. G. M. Srinivas, C. Moslonka, I. Neri, E. Penocchio, W. D. Piñeros, M. Poletti, A. Raghu, P. Raux, K. Sekimoto, and A. Soret, "Methods and conversations in (post)modern thermodynamics," *SciPost Phys. Lect. Notes*, 80 (2024).
- ²²L. Oberreiter, U. Seifert, and A. C. Barato, "Universal minimal cost of coherent biochemical oscillations," *Phys. Rev. E* **106**, 014106 (2022).
- ²³B. Remlein, V. Weissmann, and U. Seifert, "Coherence of oscillations in the weak-noise limit," *Phys. Rev. E* **105**, 064101 (2022).
- ²⁴S. G. Marehalli Srinivas, F. Avanzini, and M. Esposito, "Thermodynamics of growth in open chemical reaction networks," *Phys. Rev. Lett.* **132**, 268001 (2024).
- ²⁵S. G. Marehalli Srinivas, F. Avanzini, and M. Esposito, "Characterizing the conditions for indefinite growth in open chemical reaction networks," *Phys. Rev. E* **109**, 064153 (2024).
- ²⁶V. Voorsluijs, F. Avanzini, G. Falasco, M. Esposito, and A. Skupin, "Calcium oscillations optimize the energetic efficiency of mitochondrial metabolism," *iScience* **27**, 109078 (2024).
- ²⁷K. Yoshimura and S. Ito, "Information geometric inequalities of chemical thermodynamics," *Phys. Rev. Res.* **3**, 013175 (2021).
- ²⁸K. Yoshimura and S. Ito, "Thermodynamic uncertainty relation and thermodynamic speed limit in deterministic chemical reaction networks," *Phys. Rev. Lett.* **127**, 160601 (2021).
- ²⁹J. H. Fritz, B. Nguyen, and U. Seifert, "Stochastic thermodynamics of chemical reactions coupled to finite reservoirs: A case study for the Brusselator," *J. Chem. Phys.* **152**, 235101 (2020).
- ³⁰A. Blokhuis, D. Lacoste, and P. Gaspard, "Reaction kinetics in open reactors and serial transfers between closed reactors," *J. Chem. Phys.* **148**, 144902 (2018).
- ³¹F. Avanzini and M. Esposito, "Thermodynamics of concentration vs flux control in chemical reaction networks," *J. Chem. Phys.* **156**, 014116 (2022).
- ³²K. Ball, T. G. Kurtz, L. Popovic, and G. Rempala, "Asymptotic analysis of multiscale approximations to reaction networks," *The Annals of Applied Probability* **16**, 1925 – 1961 (2006).
- ³³S. Menz, J. C. Latorre, C. Schütte, and W. Huisinga, "Hybrid stochastic–deterministic solution of the chemical master equation," *Multiscale Modeling & Simulation* **10**, 1232–1262 (2012).

- ³⁴A. Crudu, A. Debussche, A. Muller, and O. Radulescu, "Convergence of stochastic gene networks to hybrid piecewise deterministic processes," *The Annals of Applied Probability* **22**, 1822 – 1859 (2012).
- ³⁵H.-W. Kang and T. G. Kurtz, "Separation of time-scales and model reduction for stochastic reaction networks," *The Annals of Applied Probability* **23**, 529 – 583 (2013).
- ³⁶D. Anderson and T. Kurtz, *Stochastic Analysis of Biochemical Systems*, Mathematical Biosciences Institute Lecture Series (Springer International Publishing, 2015).
- ³⁷S. Winkelmann and C. Schütte, "Hybrid models for chemical reaction networks: Multiscale theory and application to gene regulatory systems," *J. Chem. Phys.* **147**, 114115 (2017).
- ³⁸P. G. Hufton, Y. T. Lin, and T. Galla, "Model reduction methods for population dynamics with fast-switching environments: Reduced master equations, stochastic differential equations, and applications," *Phys. Rev. E* **99**, 032122 (2019).
- ³⁹H. Risken, *The Fokker-Planck Equation*, 2nd ed. (Springer-Verlag, Berlin, 1989).
- ⁴⁰H. Touchette, "The large deviation approach to statistical mechanics," *Physics Reports* **478**, 1–69 (2009).
- ⁴¹P. Bressloff, *Stochastic Processes in Cell Biology*, Interdisciplinary Applied Mathematics (Springer International Publishing, Cham, 2014).
- ⁴²H. Touchette, "Introduction to dynamical large deviations of Markov processes," *Physica A: Statistical Mechanics and its Applications* **504**, 5–19 (2018), lecture Notes of the 14th International Summer School on Fundamental Problems in Statistical Physics.
- ⁴³H. Qian and H. Ge, *Stochastic Chemical Reaction Systems in Biology* (Springer Nature, Cham, 2021).
- ⁴⁴G. Falasco and M. Esposito, "Macroscopic stochastic thermodynamics," *Rev. Mod. Phys.* **97**, 015002 (2025).
- ⁴⁵J. M. Horowitz, "Diffusion approximations to the chemical master equation only have a consistent stochastic thermodynamics at chemical equilibrium," *J. Chem. Phys.* **143**, 044111 (2015).
- ⁴⁶A. Ceccato and D. Frezzato, "Remarks on the chemical fokker-planck and langevin equations: Nonphysical currents at equilibrium," *J. Chem. Phys.* **148**, 064114 (2018).
- ⁴⁷T. G. Kurtz, "The relationship between stochastic and deterministic models for chemical reactions," *J. Chem. Phys.* **57**, 2976–2978 (1972).
- ⁴⁸Z. G. Nicolaou, T. Nishikawa, S. B. Nicholson, J. R. Green, and A. E. Motter, "Non-normality and non-monotonic dynamics in complex reaction networks," *Phys. Rev. Res.* **2**, 043059 (2020).
- ⁴⁹S. Schuster and R. Schuster, "A generalization of wegscheider's condition. implications for properties of steady states and for quasi-steady-state approximation," *J. Math. Chem.* **3**, 25–42 (1989).
- ⁵⁰A. Faggionato, D. Gabrielli, and M. Ribezzi Crivellari, "Non-equilibrium thermodynamics of piecewise deterministic markov processes," *Journal of Statistical Physics* **137**, 259–304 (2009).